Spherical optomagnonic microresonators: Triple-resonant photon transitions between Zeeman-split Mie modes

E. Almpanis,[1,2,*] G. P. Zouros,[1,3,†] P. A. Pantazopoulos,[1] K. L. Tsakmakidis,[1] N. Papanikolaou,[2] and N. Stefanou[1]

[1]*Section of Condensed Matter Physics, National and Kapodistrian University of Athens, Panepistimioupolis, GR-157 84 Athens, Greece*

[2]*Institute of Nanoscience and Nanotechnology, NCSR "Demokritos," Patriarchou Gregoriou and Neapoleos Street, Ag. Paraskevi, GR-153 10 Athens, Greece*

[3]*School of Electrical and Computer Engineering, National Technical University of Athens, GR-157 73 Athens, Greece*

(Received 24 November 2019; revised manuscript received 24 January 2020; accepted 24 January 2020; published 7 February 2020)

We report a thorough theoretical investigation of magnon-assisted photon transitions in magnetic garnet micron-sized spheres, which operate as optomagnonic resonators. In this case, matching the intraband splitting of optical Mie modes, induced by particle magnetization, to the eigenfrequency of the uniform-precession spin wave, high-efficiency triply resonant optical transitions between these modes, through respective emission or absorption of a cavity magnon, are enabled. By means of rigorous full electrodynamic computations, supported by corresponding approximate analytical calculations, we provide compelling evidence of greatly increased optomagnonic interaction, compared to that in similar processes between whispering gallery modes of corresponding submillimeter spheres, due to the reduced magnon mode volume. We explain the underlying mechanisms to a degree that goes beyond existing interpretation, invoking group theory to derive general selection rules and highlighting the role of the photon spin as the key property for maximizing the respective coupling strength.

DOI: 10.1103/PhysRevB.101.054412

I. INTRODUCTION

Tailoring and enhancing the interaction between visible/near-infrared (Vis/NIR) light and spin waves in dual, so-called optomagnonic or photomagnonic, cavities have recently attracted a lot of attention for a variety of reasons, not the least of which is the promising potential in realizing magnon-based microwave-to-optical transducers [1–3] appropriate for quantum-computing applications [4–7]. In this respect, several configurations have been proposed, including planar waveguides [2], photomagnonic crystals [8,9], and Fabry-Pérot cavities [10–16] of dielectric magnetic materials, although the most common experimentally investigated optomagnonic cavity is a millimeter-sized yttrium iron garnet (YIG) spherical particle [17–21]. The YIG sphere exhibits high-Q optical whispering gallery modes (WGMs) in the Vis/NIR part of the spectrum while, at the same time, it supports spin-wave excitations (magnons) with frequencies of 1–10 GHz. Depending on the excitation route, several magnonic modes can be triggered [22–24], the most efficiently excited one being the fundamental uniform precession, termed Kittel, mode [25,26].

When the frequency difference between two WGMs is equal to the frequency of a cavity magnon, the so-called triple-resonance condition is met, and efficient frequency up-conversion (down-conversion) of a photon can take place through the respective absorption (emission) of a magnon, provided the appropriate selection rules are satisfied. Such processes that involve three particles, i.e., two different photons and one magnon, have been probed through Brillouin light scattering experiments, measuring the corresponding Stokes or anti-Stokes scattering intensities [17–19]. However, the observed conversion efficiencies from one WGM to another, mediated by a Kittel magnon, are rather small, which limits the possibility for practical applications. The reason for this inefficient coupling between optical WGMs and the Kittel magnon is the low spatial overlap of the corresponding mode profiles; the optical field in the WGM is spatially confined to a very thin ringlike region at the boundaries of the sphere, while the Kittel magnon exhibits a spatially uniform magnetization field profile. As a result, the overlap between these modes is small, resulting in a rather weak optomagnonic effect. A possible route to enhance the optomagnonic interaction is to consider higher-order, so-called Walker, magnon modes [27–32] with a spatial distribution localized towards the resonator's boundaries, increasing in this way the overlap with the optical WGMs. Nevertheless, Walker magnons are still difficult to control, and their excitation is not as robust and efficient as that of the Kittel magnon.

An alternative route to enhance the optomagnonic interaction in magnetic spherical particles is to scale down the size of the sphere, harnessing in this way the properties of optical Mie resonances as demonstrated theoretically by Almpanis [33]. However, although the quasistatic approximation undertaken in Ref. [33] is able to predict the time variation of the scattered electromagnetic (EM) field in the presence of

*ealmpanis@gmail.com
†zouros@ieee.com

a magnonic excitation, it cannot account for energy transfer from one optical mode to another, and thus, it is not suitable to describe triple-resonant optical transitions where a nonadiabatic, fully dynamic approach should be applied [14,15]. Nevertheless, in the weak-coupling regime, which is valid in such optomagnonic resonators [17–19], magnon-mediated photon-to-photon conversion probabilities can be evaluated to first-order Born approximation, which is adequate enough for this purpose and at the same time allows for a deeper insight into the underlying physics.

In the present paper we report a thorough theoretical study of triply resonant optomagnonic interactions in a magnetic garnet microsphere. When unmagnetized, the sphere supports degenerate optical Mie modes characterized by a given polarization P [transverse electric (TE) or transverse magnetic (TM)] and a given angular momentum number $\ell = 1, 2, \ldots$. For a fixed sphere radius, the mode frequencies increase with ℓ, or, equivalently, by increasing the particle radius, modes of higher ℓ are brought into a given frequency range [34]. Specifically, at Vis/NIR frequencies, garnet microspheres exhibit Mie resonances with typical values of ℓ of the order of 10, while, for such millimeter-sized spheres, typical ℓ values for WGMs are several hundreds or thousands in that spectral range. When the spherical particle is magnetized, the $P\ell$ character of Mie modes is no longer conserved.

The magnetized micron-sized sphere exhibits nondegenerate Mie-type optical modes of different magnetic numbers $m = -\ell, -\ell+1, \ldots, \ell$ (Zeeman-like splitting) [33], as schematically shown in Fig. 1(a). In the Vis/NIR part of the EM spectrum, the frequency splitting between such neighboring modes matches the typical frequencies of magnons, i.e., a few gigahertz (GHz), so that magnon-mediated photon-to-photon transitions fulfilling the triple-resonance condition, as illustrated in Fig. 1(b), can be realized. It is worth pointing out that, for larger (millimeter-sized) particles, the triple-resonance condition is satisfied for optical transitions between successive WGMs with different predominant polarization P and angular momentum index ℓ since their frequency difference is again a few GHz. Nevertheless, for sphere radii below 100 μm the frequency difference between successive WGMs severely exceeds the magnon's frequency [35]. A further difference between our work and the descriptions reported so far [17–21,30–32] is that, here, we treat perturbatively only the action of the spin wave and not that of the static magnetization field. The latter is fully taken into account in evaluating exactly the Zeeman-split Mie modes using the rigorous coupled-field volume integral equation–Dini series expansion (CFVIE-DSE) method [36,37].

The remainder of the paper is organized as follows. In Sec. II we mention our CFVIE-DSE method, which is summarized in the Appendix, employed for the rigorous calculation of the EM field eigenmodes of a statically magnetized sphere, and analyze the symmetry of these modes in terms of group theory. In Sec. III we discuss the description of photon transitions between Zeeman-split Mie modes, induced by a uniform-precession spin wave, to first order in perturbation theory and establish the selection rules that govern such transitions. Section IV is devoted to the discussion of our results. We provide a consistent interpretation of the systematic variation of the calculated photon transition amplitudes between different modes and uncover the role of the photon spin as the key property that determines these amplitudes in Kittel-magnon-driven transitions. The last section summarizes our main findings.

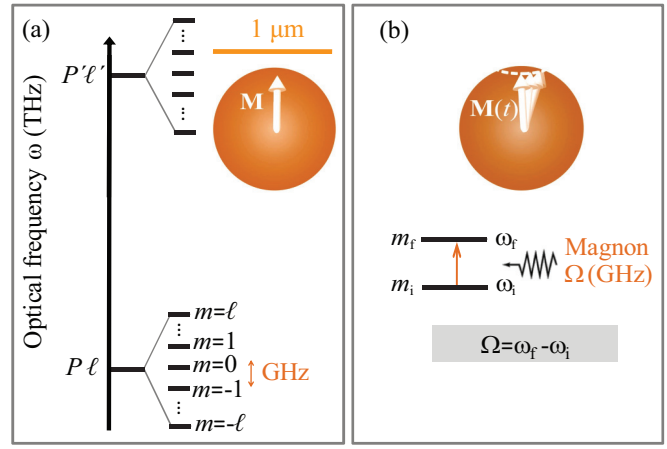

FIG. 1. (a) Schematic representation of Mie mode degeneracy lifting (Zeeman splitting) in a dielectric magnetic microsphere. In the unmagnetized sphere, these modes are characterized by a given polarization P [transverse electric or transverse magnetic] and a given angular momentum number $\ell = 1, 2, \ldots$, while they are $(2\ell+1)$-fold degenerate with respect to the magnetic number $m = -\ell, -\ell+1, \ldots, \ell$. For magnetic garnet spheres in the Vis/NIR part of the EM spectrum, Zeeman splitting can attain large values, of the order of 10 GHz. (b) Graphical illustration of the triple-resonance condition in a one-magnon absorption (photon frequency up-conversion) process: Photon transition from a mode at ω_i to a mode at ω_f by absorption of one magnon of angular frequency $\Omega = \omega_f - \omega_i$. The corresponding one-magnon emission process yields photon frequency down-conversion.

II. METHOD OF CALCULATION

Typically, magnetically saturated rare-earth iron garnets in the Vis/NIR part of the EM spectrum exhibit a gyroelectric optical response described by a relative permittivity tensor of the form

$$\bar{\bar{\epsilon}} = \begin{pmatrix} \epsilon & if & 0 \\ -if & \epsilon & 0 \\ 0 & 0 & \epsilon \end{pmatrix} \tag{1}$$

if we assume the magnetization is along the z axis, where f is the dimensionless Faraday coefficient [38] and ϵ is the relative isotropic permittivity of the unmagnetized material. The relative magnetic permeability is scalar and equals that of free space, i.e., $\mu = 1$.

In the present work we shall calculate the EM eigenmodes in a sphere of radius R made of such a magnetic material using the rigorous CFVIE-DSE method [36,37], which we briefly outline in the Appendix. This method leads to a homogeneous linear system, whose solutions are the complex eigenfrequencies of the magnetized sphere, $z_\nu = \omega_\nu - i\gamma_\nu$, $\nu = 1, 2, \ldots$, with ω_ν being the resonance frequency and γ_ν/π being the corresponding resonance linewidth, since the modes are not completely bound. Causality implies $\gamma_\nu > 0$ for $\exp(-i\omega t)$

TABLE I. Character table of the $C_{\infty h}$ point group ($m = 0, \pm1, \pm2, \ldots$). C_ϕ are rotation operations through an angle ϕ ($-\pi < \phi \leqslant \pi$), and I is the inversion operation.

$C_{\infty h}$	C_ϕ	IC_ϕ
E_{mg}	$e^{im\phi}$	$e^{im\phi}$
E_{mu}	$e^{im\phi}$	$-e^{im\phi}$

time dependence. The complex roots z_ν are retrieved by the global algorithm Complex roots Computation (CCOMP) [39].

The field distributions for each eigenmode of the magnetized sphere are retrieved from the corresponding eigenvectors, which provide the unknown field expansion coefficients [40]. It should be noted that the eigenmodes can be computed separately for every different value of m and parity $\sigma = \mathrm{g}$ (*gerade*) or $\sigma = \mathrm{u}$ (*ungerade*) of the spherical vector wave function defined in the Appendix, which remain constant because of the symmetry of the system. Therefore, in each $m\sigma$ invariant subspace, we use the index $\nu = 1, 2, \ldots$ to label the successive solutions.

In terms of group theory, the $(2\ell + 1)$ degeneracy of a Mie mode is lifted when the spherical particle is magnetized, say, along the z direction because the symmetry is reduced from $O(3)$ to $C_{\infty h}$ [41], which can be understood as a Zeeman-like splitting. Projecting onto the irreducible representations of the $C_{\infty h}$ point group, listed in Table I, one obtains $m = -\ell, -\ell + 1, \ldots, \ell$ distinct nondegenerate modes, which have E_{mg} symmetry for a TM electric multipole (N type) of even order or a TE magnetic multipole (M type) of odd order and E_{mu} symmetry for an electric multipole of odd order or a magnetic multipole of even order. This means that each Zeeman-split Mie mode is characterized by a well-defined value of m while these modes have the same parity σ and order ν, namely, those of the degenerate parent Mie modes. Consequently, they have neither a specific polarization nor a specific multipole order in the strict sense, although their dominant character is that of the parent Mie modes. The electric field intensity of these modes, similar to WGMs [42], exhibits a number of peaks along the radial direction, the meridian, and the circumference of the sphere, which equal to ν, $\ell - |m| + 1$, and m, respectively.

III. MAGNON-INDUCED PHOTON TRANSITIONS

In the previous section, we considered a statically magnetized spherical particle, where the magnetically induced gyroelectric permittivity tensor causes a Zeeman-like splitting of the optical Mie modes. However, if the magnetization dynamics comes into play, it implies a time-dependent perturbation in the dielectric permittivity tensor. In particular, for the Kittel mode, where the magnetization precesses in phase throughout the entire sphere with angular frequency Ω [26] about the z axis, forming a right circular cone with semiopening angle $\vartheta = \arctan(\eta)$, we have [33]

$$\mathbf{M}(t)/M_s = \eta\cos(\Omega t)\widehat{\mathbf{x}} + \eta\sin(\Omega t)\widehat{\mathbf{y}} + \widehat{\mathbf{z}}, \tag{2}$$

where M_s is the saturation magnetization along the z axis, and the time-dependent permittivity tensor will have the form

$$\overline{\overline{\epsilon}}(t) = \overline{\overline{\epsilon}} + \delta\overline{\overline{\epsilon}}(t). \tag{3}$$

Its static part, $\overline{\overline{\epsilon}}$, given by Eq. (1), can be written in the form

$$\overline{\overline{\epsilon}} = \epsilon\overline{\overline{I}} - f\overline{\overline{S_z}}, \tag{4}$$

while its dynamic part, $\delta\overline{\overline{\epsilon}}(t)$, reads [11]

$$\delta\overline{\overline{\epsilon}}(t) = \begin{pmatrix} 0 & 0 & -if\eta\sin(\Omega t) \\ 0 & 0 & if\eta\cos(\Omega t) \\ if\eta\sin(\Omega t) & -if\eta\cos(\Omega t) & 0 \end{pmatrix} \equiv -\frac{f\eta}{2}\left[e^{-i\Omega t}\overline{\overline{S}}_+ + e^{i\Omega t}\overline{\overline{S}}_-\right], \tag{5}$$

with $\overline{\overline{S}}_\pm = \overline{\overline{S}}_x \pm i\overline{\overline{S}}_y$, where we have made use of the spin-1 matrices [43] (in units of $\hbar$)

$$\overline{\overline{S}}_x = \begin{pmatrix} 0 & 0 & 0 \\ 0 & 0 & -i \\ 0 & i & 0 \end{pmatrix}, \quad \overline{\overline{S}}_y = \begin{pmatrix} 0 & 0 & i \\ 0 & 0 & 0 \\ -i & 0 & 0 \end{pmatrix}, \quad \overline{\overline{S}}_z = \begin{pmatrix} 0 & -i & 0 \\ i & 0 & 0 \\ 0 & 0 & 0 \end{pmatrix}. \tag{6}$$

In the weak-coupling regime, where the descriptions of optomagnonic cavities reported so far [1,10,17–19,21,29–32] are based, one can restrict the calculation to the first-order Born approximation. In this approximation, the magnon-mediated transitions are described by the overlap integral $G = \langle \mathrm{f}|\,\delta\overline{\overline{\epsilon}}\,|\mathrm{i}\rangle$, where $\langle\alpha\mathbf{r}t|\mathrm{i}\rangle = E_{\mathrm{i};\alpha}(\mathbf{r})\exp(-i\omega_\mathrm{i}t)$ and $\langle\mathrm{f}|\alpha\mathbf{r}t\rangle = E^*_{\mathrm{f};\alpha}(\mathbf{r})\exp(i\omega_\mathrm{f}t)$, with α denoting (Cartesian) component, correspond to appropriate initial (i) and final (f) EM modes of the statically magnetized sphere. As discussed in the previous section, quite generally, these modes are labeled by indices $m_\mathrm{i}\sigma_\mathrm{i}\nu_\mathrm{i}$ and $m_\mathrm{f}\sigma_\mathrm{f}\nu_\mathrm{f}$, respectively. The overlap integral, in explicit form, reads

$$G = \int dt \int_V d^3r\mathbf{E}^\dagger_\mathrm{f}(\mathbf{r})\exp(i\omega_\mathrm{f}t)\delta\overline{\overline{\epsilon}}(t)\mathbf{E}_\mathrm{i}(\mathbf{r})\exp(-i\omega_\mathrm{i}t), \tag{7}$$

where V is the volume of the sphere and the dagger denotes conjugate transpose. Substituting $\delta\overline{\overline{\epsilon}}(t)$, from Eq. (5), into Eq. (7), we obtain

$$G = \pi[\delta(\omega_\mathrm{i} - \omega_\mathrm{f} + \Omega)g_+ + \delta(\omega_\mathrm{i} - \omega_\mathrm{f} - \Omega)g_-], \tag{8}$$

where $g_+ = \langle\mathrm{f}|\delta\overline{\overline{\epsilon}}|\mathrm{i}\rangle$ and $g_- = \langle\mathrm{f}|\delta\overline{\overline{\epsilon}}^\dagger|\mathrm{i}\rangle$, which can be written in the form

$$g_\pm = if\eta\mathbf{u}_\pm \cdot \int_V d^3r\mathbf{E}^*_\mathrm{f}(\mathbf{r}) \times \mathbf{E}_\mathrm{i}(\mathbf{r}), \tag{9}$$

with $\mathbf{u}_\pm = \widehat{\mathbf{x}} \pm i\widehat{\mathbf{y}}$ and the star denoting complex conjugation. The δ functions in Eq. (8) express energy conservation in the optical transitions that involve absorption and emission of one magnon by a photon, as expected in the linear regime.

It is straightforward to show that $\mathbf{P}\delta\overline{\overline{\epsilon}}\mathbf{P}^{-1} = \exp(i\phi)\delta\overline{\overline{\epsilon}}$ and $\mathbf{P}\delta\overline{\overline{\epsilon}}^\dagger\mathbf{P}^{-1} = \exp(-i\phi)\delta\overline{\overline{\epsilon}}^\dagger$ $\forall\, P \in C_{\infty h}$, where $\mathbf{P}$ is the transformation matrix in the three-dimensional Euclidean space that corresponds to operation P. This implies (see Table I) that $\delta\overline{\overline{\epsilon}}$ and $\delta\overline{\overline{\epsilon}}^\dagger$ are irreducible tensor operators which have the

symmetry of the irreducible representations E_{1g} and E_{-1g} of $C_{\infty h}$. Therefore, $\delta\overline{\overline{\epsilon}}\,|m\sigma\nu\rangle$ and $\delta\overline{\overline{\epsilon}}^{\dagger}\,|m\sigma\nu\rangle$ transform according to the relevant direct product representations $E_{1g}\otimes E_{m\sigma} = E_{(m+1)\sigma}$ and $E_{-1g}\otimes E_{m\sigma} = E_{(m-1)\sigma}$, respectively, where $\sigma =$ g or $\sigma =$ u. These considerations imply a simple selection rule for the above photon transitions: $m_f = m_i + 1$ and $m_f = m_i - 1$ for one-magnon absorption (anti-Stokes) and one-magnon emission (Stokes) processes, respectively, while both initial and final states must have the same parity, $\sigma_f = \sigma_i$. We note that considering the corresponding magnetic point group, $D_{\infty h}(C_{\infty h})$, leads to the same selection rules. As long as, in the present work, we are concerned with transitions between Zeeman-split Mie modes, which have the same parity σ and order ν (those of the parent Mie modes), we shall denote each of the initial and final states by a single index, m_i and m_f, respectively. It should be noted that, here, we use the Dirac bra-ket notation for convenience because it allows for a more compact description of vector spaces and operations in these spaces. A similar notation has been applied to other classical fields as well, e.g., elastic waves in phononic crystals [44].

Since we are interested in transitions involving a single photon in the initial and final states, each photonic eigenmode should be appropriately normalized. For linear nondissipative and nondispersive anisotropic media [45,46], the normalization condition reads [32]

$$\frac{1}{4}\int_V d^3r[\mathbf{E}_m(\mathbf{r})\cdot\mathbf{D}_m^*(\mathbf{r}) + \mathbf{H}_m(\mathbf{r})\cdot\mathbf{B}_m^*(\mathbf{r})] = \frac{\hbar\omega_m}{2}. \quad (10)$$

Similarly, normalizing the spin-wave amplitude in Eq. (2) to correspond to one magnon (one Bohr magneton) within the volume of the sphere [32,47], we have

$$\eta = \sqrt{\frac{3\hbar|\gamma_e|}{2\pi M_s R^3}}, \quad (11)$$

where γ_e is the gyromagnetic ratio and the quantity $\hbar|\gamma_e|$ corresponds to one Bohr magneton.

IV. RESULTS AND DISCUSSION

We consider a rare-earth iron garnet spherical particle of radius $R = 0.6\,\mu$m, in air, which operates as an optomagnonic resonator. Such dielectric magnetic particles, of micron or submicron size, can be fabricated by various techniques [48–54]. In general, dielectric microparticles support complex-frequency eigenmodes of the EM field, as discussed in Sec. II, which can be excited by either free-wave coupling (scattering configuration) [33], evanescent coupling [17,18,35], or fluorescence coupling [55], although in the present work we shall not be concerned with their possible excitation. For our numerical calculations we assume a relative magnetic permeability equal to unity and for the electric permittivity tensor of Eq. (1) $\epsilon = 6.5$, and $f = -0.02$. These values are taken from available experimental data on bismuth-substituted yttrium iron garnet (Bi:YIG) close to 2.067 eV, i.e., a free-space wavelength of about 600 nm [56], and we neglect dissipative losses in order to better illustrate the analysis at stake. When the sphere is unmagnetized ($f = 0$), it supports long-lifetime, spectrally separated, multipole (2^ℓ-pole) Mie resonances of TM or TE type, which confine the field inside the particle. Here, we choose such a particular resonance, namely, the $\mathrm{TE}_{\ell=12,\nu=1}$, located at a frequency $\omega_r/2\pi = 499.546$ THz, i.e., a free-space wavelength equal to 600.13 nm. This resonance corresponds to $(2\ell+1) = 25$ degenerate modes at the same frequency, as shown with dots in Fig. 2. When the spherical particle is magnetically saturated, the corresponding Zeeman-split modes are distinguished at different frequencies, as shown by open circles in Fig. 2, with their calculated linewidth γ/π being about 0.8 GHz, which indicates the existence of high-Q spectrally separated resonances. Their separation $\Delta\omega/2\pi$ varies from 0.5 to about 10 GHz, which lies within the frequency range of Kittel resonances excited in submillimeter spherical YIG particles [18,19,23,57–60]. Of course, materials with higher (lower) Faraday coefficient, magnetized at saturation, would exhibit higher (lower) spectral separation (Zeeman splitting) between the modes.

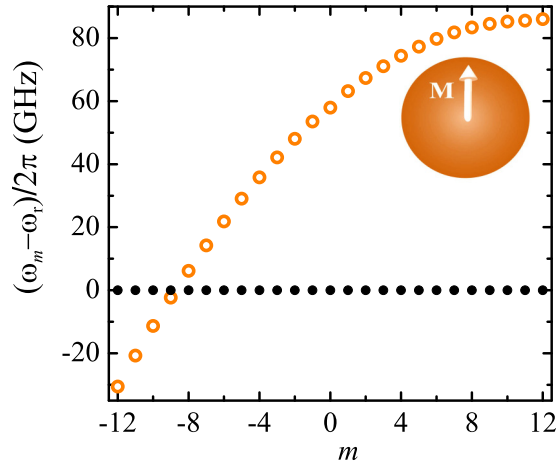

FIG. 2. Zeeman-split Mie resonance frequencies for a magnetized Bi:YIG sphere ($\epsilon = 6.5$, $f = -0.02$) of radius $R = 0.6\,\mu$m (open circles). The solid circles show the eigenfrequency ω_r of the corresponding degenerate Mie modes of the unmagnetized sphere, $\mathrm{TE}_{\ell=12,\nu=1}$, which serves as a reference for the visualization of level splitting on the GHz scale.

We now calculate the transition amplitude upon one-magnon absorption g_+, given by Eq. (9), between all successive initial, $|m_i\rangle$, and final, $|m_f\rangle$, Zeeman-split Mie modes complying with the selection rule $m_f = m_i + 1$, assuming that the magnon frequency fulfills the triple-resonance condition $\omega_f = \omega_i + \Omega$. The spin-wave amplitude is $\eta \simeq 2\times 10^{-5}$, as obtained from Eq. (11) substituting the gyromagnetic ratio $|\gamma_e|/2\pi = 28$ GHz/T and the saturation magnetization $M_s = 120$ kA/m for Bi:YIG [61–63]. The results for the optomagnonic coupling strength $\widetilde{g}_+ \equiv \epsilon_0|g_+|/\hbar$ scaled with f, depicted in Fig. 3(a), exhibit a parabolic-like behavior with a maximum at a particular value of m_i. By decreasing the magnitude of the Faraday coefficient, the position of the maximum moves towards $m_i = 0$, as shown in Fig. 3(b). Upon magnetization reversal, the Faraday coefficient changes sign, as the magnetic indices m do, since we keep the z axis fixed. Noting that the time-reversed process is a photon transition from state $|-m_i - 1\rangle$ to $|-m_i\rangle$ through emission of one magnon, reversibility

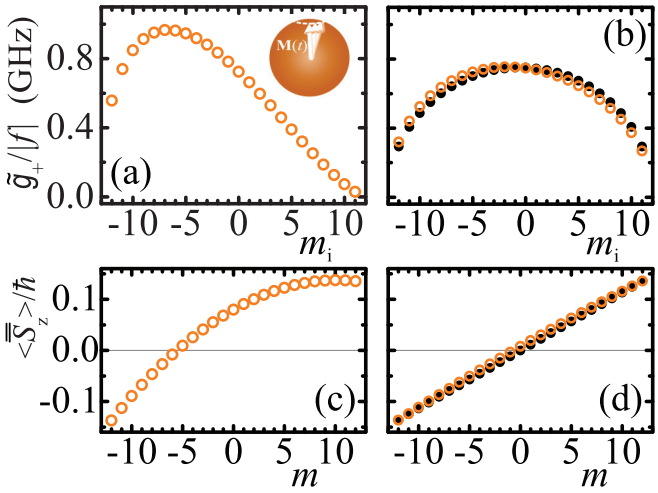

FIG. 3. (a) Calculated magnitude of the reduced optomagnonic coupling strength, $\tilde{g}_+/|f| = |g_+|\epsilon_0/(\hbar|f|)$, for triple-resonant photon transitions from the $|m_i\rangle$ to the $|m_i+1\rangle$ Zeeman-split Mie-TE$_{\ell=12,\nu=1}$ modes of a magnetized Bi:YIG sphere ($\epsilon = 6.5$, $f = -0.02$) of radius $R = 0.6\,\mu$m (see Fig. 2), induced by absorption of a Kittel magnon. (b) Respective reduced optomagnonic coupling strengths in the limit $f \to 0$ obtained analytically (dots) and calculated numerically for $f = -0.002$ (open circles). (c) and (d) Corresponding expectation value of the z component of the photon spin in each mode.

implies $|g_+(m_i, f)| = |g_-(-m_i - 1, -f)| = |g_+(-m_i, -f)|$ that expresses the symmetry of the optomagnonic coupling strength with respect to magnetization reversal.

To gain physical insight into the systematic variation of the reduced optomagnonic coupling strength, one can consider the low magneto-optical coupling limit, $f \to 0$, where an approximate analytical solution can be obtained. In this limit, to first-order approximation, instead of the Zeeman-split Mie modes of the magnetic sphere, one can employ the corresponding unsplit (degenerate) modes of the unmagnetized sphere. We recall that the EM field associated with the parent TE$_{\ell=12,\nu=1}$ Mie modes is given by

$$\begin{aligned}\mathbf{E}^M_{\ell m}(\mathbf{r}) &= a^M_{\ell m}\mathbf{M}_{\ell m}(k_r, \mathbf{r}),\\ \mathbf{H}^M_{\ell m}(\mathbf{r}) &= \frac{-i}{k_r}\sqrt{\frac{\epsilon_0\epsilon}{\mu_0}}\nabla \times \mathbf{E}^M_{\ell m}(\mathbf{r})\\ &= -ia^M_{\ell m}\sqrt{\frac{\epsilon_0\epsilon}{\mu_0}}\mathbf{N}_{\ell m}(k_r, \mathbf{r}),\end{aligned} \tag{12}$$

where $k_r = \omega_r\sqrt{\epsilon_0\epsilon\mu_0}$ is the corresponding wave number and the spherical vector wave functions are defined in the Appendix. The magnitude of the field amplitude $|a^M_{\ell m}|$ entering in Eqs. (12) is obtained from the normalization to the vacuum energy of the photon field according to Eq. (10), which, using standard properties of the spherical Bessel functions, yields

$$|a^M_{\ell m}|^2 = \frac{2\hbar\omega_r}{\epsilon_0\epsilon\ \ell(\ell+1)R^3}\left[\frac{x^3}{x^3\left[j^2_\ell(x) - j_{\ell-1}(x)j_{\ell+1}(x)\right] + x^2 j_\ell(x)j_{\ell-1}(x) - x\ell j^2_\ell(x)}\right]_{x=k_rR}. \tag{13}$$

The transition amplitude from an initial state $|m_i\rangle$ to a final state $|m_i+1\rangle$, through one-magnon absorption, given in Eq. (9), can now be expressed in closed form through

$$\begin{aligned}\left.\frac{g_+}{f\eta}\right|_{f\to 0} &= \frac{-\hbar\omega_r\sqrt{(\ell - m_i)(\ell + m_i + 1)}}{\epsilon_0\epsilon\ \ell(\ell+1)}\\ &\times\left[\frac{(2\ell+1)^2\left[j^2_\ell(x) - j_{\ell-1}(x)j_{\ell+1}(x)\right]}{(2\ell+1)^2 j^2_\ell(x) - 4\ell(\ell+1)j_{\ell-1}(x)j_{\ell+1}(x) + (\ell+1)j^2_{\ell-1}(x) - \ell j^2_{\ell+1}(x)}\right]_{x=k_rR}.\end{aligned} \tag{14}$$

This analytical formula nicely reproduces the results of the exact numerical calculations at low values of the Faraday coefficient, as shown in Fig. 3(b), enabling one to treat spheres characterized by a low Faraday coefficient as if they were unmagnetized.

At this point, it is also insightful to evaluate the expectation value of the photon spin [43,64,65] at the given TE Mie modes

$$\langle\overline{\overline{\mathbf{S}}}\rangle^M_{\ell m} = \frac{\epsilon_0\epsilon}{2i\omega_r}\int_V d^3r\left[\mathbf{E}^{M*}_{\ell m}(\mathbf{r}) \times \mathbf{E}^M_{\ell m}(\mathbf{r}) + \frac{\mu_0}{\epsilon_0\epsilon}\mathbf{H}^{M*}_{\ell m}(\mathbf{r}) \times \mathbf{H}^M_{\ell m}(\mathbf{r})\right], \tag{15}$$

which, after some lengthy but straightforward algebra, gives

$$\langle\overline{\overline{\mathbf{S}}}\rangle^M_{\ell m} = \frac{\hbar m}{\ell(\ell+1)}\left[\frac{(2\ell+1)^2 j^2_\ell(x) + [(\ell+1)j_{\ell-1}(x) - \ell j_{\ell+1}(x)]^2}{(2\ell+1)^2 j^2_\ell(x) - 4\ell(\ell+1)j_{\ell-1}(x)j_{\ell+1}(x) + (\ell+1)j^2_{\ell-1}(x) - \ell j^2_{\ell+1}(x)}\right]_{x=k_rR}\hat{\mathbf{z}}. \tag{16}$$

It should be pointed out that the indices ℓm, which characterize the spherical vector wave functions, are associated with the total angular momentum $\mathbf{J} = \mathbf{L} + \mathbf{S}$, where $\mathbf{S}$ is the spin angular momentum ($S = 1$ for photons), and not with the orbital angular momentum $\mathbf{L}$ [66]. The expectation value of the z component of the photon spin in the Mie modes under consideration, evaluated using Eq. (16), agrees perfectly with the results of rigorous numerical calculations for a magnetized sphere with low f, as shown in Fig. 3(d). An interesting observation is that, in the limit $f \to 0$, the reduced optomagnonic coupling rate takes its highest value at $m_i = 0$ or at $m_i = -1$, i.e., when the expectation value of

the z component of the photon spin in either the initial or final state, respectively, vanishes, which suggests a heuristic interpretation: As discussed in Sec. III, $g_\pm$ are essentially given by the matrix element of the x and y components of the photon spin operator between the initial and final states. Given that the spin magnitude remains constant (it equals 1 for photons), the reduced optomagnonic coupling strength should exhibit a maximum when the expectation value of the z component of the spin in the states involved becomes vanishingly small. This is indeed confirmed by our numerical calculations also for the magnetized sphere, as shown in Fig. 3(c). In the magnetized sphere, say, along the positive z direction ($f < 0$), according to Eq. (4), there is a positive contribution $-f\overline{\overline{S_z}}$ to the electric permittivity tensor. Our rigorous full electrodynamic calculations show that this intrinsic material polarization increases the expectation value of the z component of the photon spin at a given mode m by an amount proportional to the material's gyrotropy, quantified by the Faraday coefficient. As a result, the $\langle\overline{\overline{S_z}}\rangle$-versus-$m$ curve in Fig. 3(d) shifts upwards, as shown in Fig. 3(c), and therefore $\langle\overline{\overline{S_z}}\rangle$ vanishes at a negative value of m. This implies a corresponding shift of the maximum of the reduced optomagnonic coupling strength, as shown in Fig. 3(a). The opposite happens if we reverse the magnetization direction, which corresponds to positive values of f. Let us denote by m_0 the point at which $\langle\overline{\overline{S_z}}\rangle$ vanishes, as obtained, e.g., by linear interpolation between the successive (integer) values of m where $\langle\overline{\overline{S_z}}\rangle$ changes sign. On the basis of the above discussion, m_0 is expected to increase with f. This is indeed confirmed by our rigorous numerical calculations, as shown in Fig. 4. It can be seen that, interestingly, m_0 varies linearly with f for $|f| < 0.01$.

So far, we have considered triply resonant optical transitions at visible frequencies between Zeeman-split Mie modes of a dielectric magnetic microsphere, driven by Kittel magnons, which satisfy the appropriate selection rules. It would be now interesting to compare the calculated efficiencies, depicted in Fig. 3, with those attained in corresponding larger spheres, where the triple-resonance condition is met between successive optical WGMs. In the low magneto-optical coupling regime, $|f| \ll 1$, which is typical in the relevant literature [17–19], we can derive closed-form analytic expressions for such transitions as well. We note that in that case, parity invariance, implied by the general selection rules deduced in Sec. III, translates to polarization conversion along with an increase or decrease of ℓ by one unit, while $m_\mathrm{f} = m_\mathrm{i} \pm 1$. For example, for an optical transition from an initial (TM, ℓ, m) mode to a final (TE, $\ell+1, m+1$) mode, we obtain

$$\frac{g_+}{f\eta} = i a^M_{\ell+1 m+1}\, a^N_{\ell m} \times \frac{\ell(\ell+2)\sqrt{(\ell+m+1)(\ell+m+2)}}{\sqrt{(2\ell+1)(2\ell+3)}} I_\mathrm{rad}(R), \quad (17)$$

where

$$I_\mathrm{rad}(R) = \frac{R^2}{k_M^2 - k_N^2}[k_N j_{\ell+1}(k_M r) j_\ell(k_N r) - k_M j_{\ell+1}(k_N r) j_\ell(k_M r)], \quad (18)$$

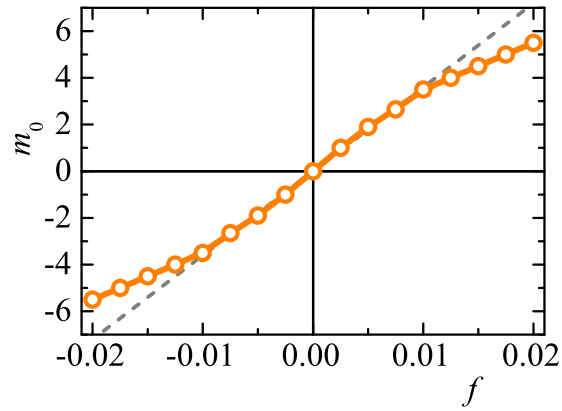

FIG. 4. A magnetic Bi:YIG sphere of radius $R = 0.6\,\mu$m, with relative permittivity $\epsilon = 6.5$ and variable Faraday coefficient ranging from $f = -0.02$ to $f = 0.02$. For each value of f, we determine the point m_0 at which the expectation value of the z component of the photon spin $\langle\overline{\overline{S_z}}\rangle$ vanishes by linear interpolation between the successive Zeeman-split $\mathrm{TE}_{\ell=12,\nu=1}$-Mie modes $|m\rangle$, where $\langle\overline{\overline{S_z}}\rangle$ changes sign. The plot displays the variation of m_0 with f. The dashed line is a guide to the eye marking the linear variation.

with $|a^N_{\ell m}| = |a^M_{\ell m}|$ given by Eq. (13) and k_M, k_N being the wave numbers of the respective modes. For spheres with radii similar to those used in relevant experiments [1,17–19,24,35], i.e., ranging from 200 to 500 μm, the normalized spin-wave amplitude η is of the order of 10^{-9}, and assuming $m = \ell$ for the WGMs [32], we obtain $\widetilde{g}_+/|f| \sim 1$ MHz at the frequencies under consideration, which is almost three orders of magnitude smaller than the maximum values of $\widetilde{g}_+/|f|$ in Fig. 3(b). Therefore, the operation of magnetic garnet microspheres as optomagnonic resonators, proposed in the present work, exhibits significantly stronger coupling between Vis/NIR photons and magnons. Even for moderate values of f, which are appropriate for NIR frequencies where optical losses are vanishingly small [67], for instance, $f = -0.002$, the optomagnonic coupling strength $\widetilde{g}_+$ can be as large as 1 MHz.

V. CONCLUSIONS

In summary, we carried out a thorough theoretical study of triply resonant photon transitions between Zeeman-split Mie modes, driven by a uniform-precession spin wave, in magnetic garnet microspheres. After deriving rigorous selection rules based on general group theory considerations, we evaluated the corresponding transition amplitudes to first-order Born approximation by accurate full electrodynamic computations. The observed systematic variation of the transition amplitude was consistently explained using the concept of the photon spin in the states involved. Due to the significantly reduced magnon mode volume, the predicted optomagnonic coupling strengths are almost three orders of magnitude larger than those expected in corresponding transitions between WGMs of respective (sub)millimeter-sized resonators as reported in the relevant literature. These findings were also supported, and further elucidated, by approximate analytical calculations based on closed-form formulas that we derived in the low

magneto-optical coupling limit. Our results suggest a viable way forward for realizing high-efficiency optomagnonic micron-sized resonators.

ACKNOWLEDGMENTS

Fruitful discussions with Dr. S. Viola Kusminskiy are acknowledged. E.A., G.P.Z., and K.L.T. were supported by the General Secretariat for Research and Technology (GSRT) and the Hellenic Foundation for Research and Innovation (HFRI) under Grant No. 1819. P.A.P. was supported by GSRT and HFRI through a Ph.D. scholarship (No. 906).

E.A. and G.P.Z. contributed equally to this work.

APPENDIX

For the Mie eigenmode problem considered here, we set a null external excitation, and the CFVIE-DSE, assuming time dependence of the $\exp(-i\omega t)$ form, becomes

$$\begin{bmatrix}\mathbf{E}(\mathbf{r})\\ \mathbf{H}(\mathbf{r})\end{bmatrix}-\begin{bmatrix}k_0^2\bar{\bar{I}}+\nabla\nabla\cdot\\ -ik_0\sqrt{\frac{\epsilon_0}{\mu_0}}\nabla\times\end{bmatrix}\int_V d^3r' g(\mathbf{r}-\mathbf{r}')(\bar{\bar{\epsilon}}-\bar{\bar{I}})\,\mathbf{E}(\mathbf{r}')=0, \tag{A1}$$

where V is the volume of the sphere; $\mathbf{E}(\mathbf{r})$ and $\mathbf{H}(\mathbf{r})$ are the total electric and magnetic fields valid at any point $\mathbf{r}$ inside and outside the resonator; $k_0=\omega\sqrt{\epsilon_0\mu_0}$ is the free-space wave number, with ϵ_0 and μ_0 being the free-space permittivity and permeability, respectively; $\bar{\bar{I}}$ is the unity dyadic; and $g(\mathbf{r},\mathbf{r}')$ is the free-space Green's function. Next, the electric and magnetic fields are expanded into linear combinations of Dini-type spherical vector wave functions (SVWFs) [36]

$$\begin{aligned}\begin{bmatrix}\mathbf{E}(\mathbf{r})\\ \mathbf{H}(\mathbf{r})\end{bmatrix}=\sum_{\ell,m,j}&\begin{bmatrix}\Gamma_{\ell mj}\\ \Sigma_{\ell mj}\end{bmatrix}\mathbf{M}_{\ell m}\big(\kappa^M_{\ell mj},\mathbf{r}\big)+\begin{bmatrix}\Delta_{\ell mj}\\ T_{\ell mj}\end{bmatrix}\mathbf{N}_{\ell m}\big(\kappa^N_{\ell mj},\mathbf{r}\big)\\&+\begin{bmatrix}Z_{\ell mj}\\ \Pi_{\ell mj}\end{bmatrix}\mathbf{L}_{\ell m}\big(\kappa^L_{\ell mj},\mathbf{r}\big),\end{aligned} \tag{A2}$$

with $\Gamma_{\ell mj}$, $\Delta_{\ell mj}$, $Z_{\ell mj}$, $\Sigma_{\ell mj}$, $T_{\ell mj}$, and $\Pi_{\ell mj}$ being unknown expansion coefficients. The corresponding SVWFs are defined as

$$\mathbf{M}_{\ell m}\big(\kappa^M_{\ell mj},\mathbf{r}\big)=\nabla\times\mathbf{r}\,j_\ell\big(\kappa^M_{\ell mj}r\big)Y_{\ell m}(\theta,\phi), \tag{A3}$$

$$\mathbf{N}_{\ell m}\big(\kappa^N_{\ell mj},\mathbf{r}\big)=\frac{1}{\kappa^N_{\ell mj}}\nabla\times\nabla\times\mathbf{r}\,j_\ell\big(\kappa^N_{\ell mj}r\big)Y_{\ell m}(\theta,\phi), \tag{A4}$$

$$\mathbf{L}_{\ell m}\big(\kappa^L_{\ell mj},\mathbf{r}\big)=\frac{1}{\kappa^L_{\ell mj}}\nabla\, j_\ell\big(\kappa^L_{\ell mj}r\big)Y_{\ell m}(\theta,\phi), \tag{A5}$$

where j_ℓ are the spherical Bessel functions and $Y_{\ell m}$ are the orthonormal spherical harmonics [68]. The Dini-type wave numbers $\kappa^M_{\ell mj}$, $\kappa^N_{\ell mj}$ are selected to establish orthogonality of $\mathbf{M}_{\ell m}$ and $\mathbf{N}_{\ell m}$ within the volume V, while $\kappa^L_{\ell mj}$ are chosen to ensure decoupling between $\mathbf{N}_{\ell m}$ and $\mathbf{L}_{\ell m}$ in V, i.e., $\langle\mathbf{N}_{\ell m}|\mathbf{L}_{\ell m}\rangle=0$ [36]. The corresponding expansions for the electric displacement $\mathbf{D}(\mathbf{r})=\epsilon_0\bar{\bar{\epsilon}}\mathbf{E}(\mathbf{r})$ and magnetic flux density $\mathbf{B}(\mathbf{r})=\mu_0\mathbf{H}(\mathbf{r})$ involve only the divergenceless $\mathbf{M}_{\ell m}$ and $\mathbf{N}_{\ell m}$ SVWFs because in a region free of charges $\nabla\cdot\mathbf{D}=0$, while $\nabla\cdot\mathbf{B}=0$ [37].

As a concluding remark, we stress that our established CFVIE-DSE method was recently applied and compared with the discrete eigenfunction method [69] in Refs. [40,42] for studying various complex resonances in combined perfectly electric conducting anisotropic spheres, including magnetic plasmon resonances in ferromagnetic resonators, and WGMs in semiconductor nanospheres.

[1] R. Hisatomi, A. Osada, Y. Tabuchi, T. Ishikawa, A. Noguchi, R. Yamazaki, K. Usami, and Y. Nakamura, Phys. Rev. B **93**, 174427 (2016).

[2] M. Kostylev and A. A. Stashkevich, J. Magn. Magn. Mater. **484**, 329 (2019).

[3] N. J. Lambert, A. Rueda, F. Sedlmeir, and H. G. Schwefel, Adv. Quantum Technol. **3**, 1900077 (2020).

[4] Y. Tabuchi, S. Ishino, A. Noguchi, T. Ishikawa, R. Yamazaki, K. Usami, and Y. Nakamura, Science **349**, 405 (2015).

[5] D. Lachance-Quirion, Y. Tabuchi, S. Ishino, A. Noguchi, T. Ishikawa, R. Yamazaki, and Y. Nakamura, Sci. Adv. **3**, e1603150 (2017).

[6] D. Lachance-Quirion, Y. Tabuchi, A. Gloppe, K. Usami, and Y. Nakamura, Appl. Phys. Express **12**, 070101 (2019).

[7] V. A. S. V. Bittencourt, V. Feulner, and S. V. Kusminskiy, Phys. Rev. A **100**, 013810 (2019).

[8] J. W. Kłos, M. Krawczyk, Y. S. Dadoenkova, N. N. Dadoenkova, and I. L. Lyubchanskii, J. Appl. Phys. **1115**, 174311 (2014).

[9] Y. S. Dadoenkova, N. N. Dadoenkova, I. L. Lyubchanskii, J. W. Kłos, and M. Krawczyk, J. Appl. Phys. **120**, 073903 (2016).

[10] T. Y. Liu, X. F. Zhang, H. X. Tang, and M. E. Flatté, Phys. Rev. B **94**, 060405(R) (2016).

[11] P. A. Pantazopoulos, N. Stefanou, E. Almpanis, and N. Papanikolaou, Phys. Rev. B **96**, 104425 (2017).

[12] P. A. Pantazopoulos, N. Papanikolaou, and N. Stefanou, J. Opt. **21**, 015603 (2018).

[13] M. A. Kozhaev, A. I. Chernov, D. A. Sylgacheva, A. N. Shaposhnikov, A. R. Prokopov, V. N. Berzhansky, A. K. Zvezdin, and V. I. Belotelov, Sci. Rep. **8**, 11435 (2018).

[14] P. A. Pantazopoulos and N. Stefanou, Phys. Rev. B **99**, 144415 (2019).

[15] P. A. Pantazopoulos, K. L. Tsakmakidis, E. Almpanis, G. P. Zouros, and N. Stefanou, New J. Phys. **21**, 095001 (2019).

[16] T. S. Parvini, V. A. S. V. Bittencourt, and S. V. Kusminskiy, arXiv:1908.06110.

[17] A. Osada, R. Hisatomi, A. Noguchi, Y. Tabuchi, R. Yamazaki, K. Usami, M. Sadgrove, R. Yalla, M. Nomura, and Y. Nakamura, Phys. Rev. Lett. **116**, 223601 (2016).

[18] X. Zhang, N. Zhu, C.-L. Zou, and H. X. Tang, Phys. Rev. Lett. **117**, 123605 (2016).

[19] J. A. Haigh, A. Nunnenkamp, A. J. Ramsay, and A. J. Ferguson, Phys. Rev. Lett. **117**, 133602 (2016).

[20] S. Viola Kusminskiy, H. X. Tang, and F. Marquardt, Phys. Rev. A **94**, 033821 (2016).

[21] S. Sharma, Y. M. Blanter, and G. E. W. Bauer, Phys. Rev. B **96**, 094412 (2017).

[22] X. Zhang, C.-L. Zou, L. Jiang, and H. X. Tang, Phys. Rev. Lett. **113**, 156401 (2014).

[23] R. G. E. Morris, A. F. van Loo, S. Kosen, and A. D. Karenowska, Sci. Rep. **7**, 11511 (2017).

[24] A. Gloppe, R. Hisatomi, Y. Nakata, Y. Nakamura, and K. Usami, Phys. Rev. Appl. **12**, 014061 (2019).

[25] C. Kittel, Phys. Rev. **73**, 155 (1948).

[26] D. D. Stancil and A. Prabhakar, *Spin Waves-Theory and Applications* (Springer, Boston, 2009).

[27] L. R. Walker, Phys. Rev. **105**, 390 (1957).

[28] P. C. Fletcher and R. O. Bell, J. Appl. Phys. **30**, 687 (1959).

[29] A. Osada, A. Gloppe, R. Hisatomi, A. Noguchi, R. Yamazaki, M. Nomura, Y. Nakamura, and K. Usami, Phys. Rev. Lett. **120**, 133602 (2018).

[30] A. Osada, A. Gloppe, Y. Nakamura, and K. Usami, New J. Phys. **20**, 103018 (2018).

[31] J. A. Haigh, N. J. Lambert, S. Sharma, Y. M. Blanter, G. E. W. Bauer, and A. J. Ramsay, Phys. Rev. B **97**, 214423 (2018).

[32] S. Sharma, B. Z. Rameshti, Y. M. Blanter, and G. E. W. Bauer, Phys. Rev. B **99**, 214423 (2019).

[33] E. Almpanis, Phys. Rev. B **97**, 184406 (2018).

[34] C. C. Lam, P. T. Leung, and K. Young, J. Opt. Soc. Am. B **9**, 1585 (1992).

[35] J. A. Haigh, S. Langenfeld, N. J. Lambert, J. J. Baumberg, A. J. Ramsay, A. Nunnenkamp, and A. J. Ferguson, Phys. Rev. A **92**, 063845 (2015).

[36] G. P. Zouros and G. C. Kokkorakis, IEEE Trans. Antennas Propag. **63**, 2665 (2015).

[37] G. P. Zouros and G. C. Kokkorakis, IEEE Trans. Microwave Theory Tech. **63**, 3054 (2015).

[38] L. D. Landau and E. M. Lifshitz, *Electrodynamics of Continuous Media* (Pergamon, Oxford, 1960).

[39] G. P. Zouros, Comput. Phys. Commun. **222**, 339 (2018).

[40] G. P. Zouros, G. D. Kolezas, and I. G. Kyrannas, IEEE Trans. Antennas Propag. **66**, 5282 (2018).

[41] T. Inui, Y. Tanabe, and Y. Onodera, *Group Theory and Its Applications in Physics* (Springer, Berlin, 1990).

[42] G. P. Zouros, J. Appl. Phys. **124**, 174301 (2018).

[43] M. V. Berry, J. Opt. A **11**, 094001 (2009).

[44] R. Sainidou, N. Stefanou, and A. Modinos, Phys. Rev. B **69**, 064301 (2004).

[45] R. Ruppin, Phys. Lett. A **299**, 309 (2002)

[46] F. D. Nunes, T. C. Vasconcelos, M. Bezerra, and J. Weiner, J. Opt. Soc. Am. B **28**, 1544 (2011).

[47] J. Graf, H. Pfeifer, F. Marquardt, and S. Viola Kusminskiy, Phys. Rev. B **98**, 241406(R) (2018).

[48] G. C. Stangle, K. R. Venkatachari, S. P. Ostrander, W. A. Schulze, and J. D. Pietras, US Patent No. 5,660,773 (1997).

[49] M. Jafelicci, Jr., and R. H. M. Godoi, J. Magn. Magn. Mater. **226**, 1421 (2001).

[50] F. Grasset, S. Mornet, A. Demourgues, J. Portier, J. Bonnet, A. Vekris, and E. Duguet, J. Magn. Magn. Mater. **234**, 409 (2001).

[51] Y. J. Wu, H. P. Fu, R. Y. Hong, Y. Zheng, and D. G. Wei, J. Alloys Compd. **470**, 497 (2009).

[52] R. Y. Hong, Y. J. Wu, B. Feng, G. Q. Di, H. Z. Li, B. Xud, Y. Zheng, and D. G. Wei, J. Magn. Magn. Mater. **321**, 1106 (2009).

[53] C. L. Sones, M. Feinaeugle, A. Sposito, B. Gholipour, and R. W. Eason, Opt. Express **20**, 15171 (2012).

[54] T. Schmitz, U. Wiedwald, C. Dubs, and B. Gökce, Chem. Phys. Chem. **18**, 1125 (2017).

[55] M. Kuwata-gonokami, K. Ema, and K. Takeda, Mol. Cryst. Liq. Cryst. Sci. Technol., Sect. A **216**, 21 (1992).

[56] V. Doormann, J.-P. Krumme, and H. Lenz, J. Appl. Phys. **68**, 3544 (1990).

[57] S. Kaur, B. M. Yao, J. W. Rao, Y. S. Gui, and C.-M. Hu, Appl. Phys. Lett. **109**, 032404 (2016).

[58] C. Braggio, G. Carugno, M. Guarise, A. Ortolan, and G. Ruoso, Phys. Rev. Lett. **118**, 107205 (2017).

[59] J. W. Rao, B. M. Yao, X. L. Fan, D. S. Xue, Y. S. Gui, and C. M. Hu, Appl. Phys. Lett. **112**, 262401 (2018).

[60] R. Hisatomi, A. Noguchi, R. Yamazaki, Y. Nakata, A. Gloppe, Y. Nakamura, and K. Usami, Phys. Rev. Lett. **123**, 207401 (2019).

[61] T. Hirano, H. Hotaka, E. Komuro, T. Namikawa, and Y. Yamazaki, IEEE Trans. Magn. **28**, 3237 (1992).

[62] H. Kidoh, H. Yashima, A. Morimoto, and T. Shimizu, Jpn. J. Appl. Phys. **33**, 4094 (1994).

[63] S. E. Irvine and A. Y. Elezzabi, Proc. SPIE **5260**, 585 (2003).

[64] S. J. van Enk and G. Nienhuis, Opt. Commun. **94**, 147 (1992).

[65] K. Y. Bliokh, A. Y. Bekshaev, and F. Nori, Phys. Rev. Lett. **119**, 073901 (2017).

[66] L. Dai, M. Kamionkowski, and D. H. Jeong, Phys. Rev. D **86**, 125013 (2012).

[67] A. Zvezdin and V. Kotov, *Modern Magnetooptics and Magnetooptical Materials* (Institute of Physics Publishing, Bristol, United Kingdom, 1997).

[68] J. D. Jackson, *Classical Electrodynamics* (Wiley, New York, 1999).

[69] J. L. W. Li and W. L. Ong, IEEE Trans. Antennas Propag. **59**, 3370 (2011).